

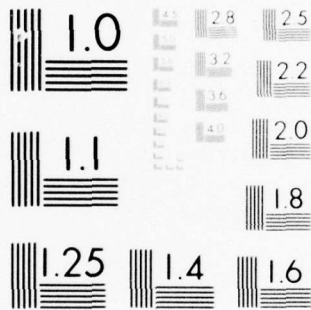
AD-A045 015

NATIONAL WEATHER SERVICE SILVER SPRING MD TECHNIQUES --ETC F/G 4/2
THUNDERSTORM PREDICTION FOR USE IN AIR TRAFFIC CONTROL (0-6 HOU--ETC(U)
JUL 77 M A ALAKA, J P CHARBA, R C ELVANDER DOT-FA74WAI-488
FAA-RD-77-40 NL

UNCLASSIFIED

| OF |
AD
A045015





Report No. FAA-RD-77-40

[Handwritten signature] **12**

AD A 045015

THUNDERSTORM PREDICTION FOR USE IN AIR TRAFFIC CONTROL (0-6 Hours Time Range)

M.A. Alaka, J.P. Charba, and R.C. Elvander
National Weather Service
National Oceanic and Atmospheric Administration
U.S. Department of Commerce
Silver Spring, Md. 20910



July 1977
FINAL REPORT

DDC
RECEIVED
OCT 11 1977
[Handwritten signature] **C**

Document is available to the U.S. public through
the National Technical Information Service,
Springfield, Virginia 22161

AD No. _____
DDC FILE COPY.

Prepared for
U.S. DEPARTMENT OF TRANSPORTATION
FEDERAL AVIATION ADMINISTRATION
Systems Research & Development Service
Washington, D.C. 20590

12

THUNDERSTORM PREDICTION
FOR USE IN AIR TRAFFIC CONTROL

NOTICE

This document is disseminated under the sponsorship of the Department of Transportation in the interest of information exchange. The United States Government assumes no liability for its contents or use thereof.

National Weather Service
National Oceanic and Atmospheric Administration
U.S. Department of Commerce
Silver Spring, Md. 20910



July 1977
FINAL REPORT

RECEIVED
OCT 11 1977
D.D.C.

Document is available to the U.S. public through
the National Technical Information Service
Springfield, Virginia 22161

Prepared for
U.S. DEPARTMENT OF TRANSPORTATION
FEDERAL AVIATION ADMINISTRATION
Systems Research & Development Service
Washington, D.C. 20586

Technical Report Documentation Page

1. Report No. 19 18 FAA-RD-77-48	2. Government Accession No.	3. Recipient's Catalog No.
4. Title and Subtitle 6 Thunderstorm Prediction for Use in Air Traffic Control (0-6 Hours Time Range)	5. Report Date 11 July 1977	6. Performing Organization Code
7. Author(s) 10 M. A. Alaka, J. P. Charba, and R. C. Elvander	8. Performing Organization Report No. 12 36p.	9. Report Date
9. Performing Organization Name and Address Techniques Development Laboratory Systems Development Office NOAA, National Weather Service U.S. Dept. of Commerce, Silver Spring, MD 20910	10. Work Unit No. (TRAIS)	11. Contract or Grant No. 15 Interagency Agreement DOT-FA74WAT-488
12. Sponsoring Agency Name and Address Department of Transportation Federal Aviation Administration Systems Research & Development Service, Airport Div. Aviation Weather Systems Branch, Washington, DC 20591	13. Type of Report and Period Covered 9 Final Report September 1975-January 1977	14. Sponsoring Agency Code
15. Supplementary Notes		
<p>16. Abstract</p> <p>→ This report updates results, described in a previous interim report, of our efforts to develop short range (0-6 hr) thunderstorm forecasts for aviation.</p> <p><i>we made</i> In the 0-2 hr range, we have made systematic comparisons of the capabilities of three techniques of varying complexity in predicting the movement of radar echoes associated with thundery activity. We used 10- and 30-minute data sequences of radar data to produce 10-, 30-, 60-, and 90-minute forecasts. Our results show that in general, the complex technique has little advantage over simple techniques which can be implemented locally on the mini-computer.</p> <p><i>Jan- and were used to produce</i></p> <p>In the 2-6 hr range, we have used a combination of classical and model output statistics (MOS) to develop probability forecasts of thunderstorm activity over most of the U. S. east of the Rockies. Forecasts valid for the periods 1700-2100, 2000-0000, and 2300-0300 GMT are now available for the spring and summer seasons and are being transmitted to the field three times daily by teletype. <i>we used</i></p>		
17. Key Words Thunderstorm Prediction Probability Forecasting Echo Tracking, Radar Data Vertical-Integrated Liquid-Water Content		18. Distribution Statement Document is available to the public through the National Technical Information Service, Springfield, Virginia 22151.
19. Security Classif. (of this report) Unclassified	20. Security Classif. (of this page) Unclassified	21. No. of Pages 32
		22. Price

METRIC CONVERSION FACTORS

Approximate Conversions to Metric Measures

Symbol	When You Know	Multiply by	To Find	Symbol
LENGTH				
in	inches	2.5	centimeters	cm
ft	feet	30	centimeters	cm
yd	yards	0.9	meters	m
mi	miles	1.6	kilometers	km
AREA				
sq in	square inches	6.5	square centimeters	cm ²
sq ft	square feet	0.09	square meters	m ²
sq yd	square yards	0.8	square meters	m ²
sq mi	square miles	2.6	square kilometers	km ²
acres	acres	0.4	hectares	ha
MASS (weight)				
oz	ounces	28	grams	g
lb	pounds	0.45	kilograms	kg
	short tons (2000 lb)	0.9	tonnes	t
VOLUME				
teaspoons	teaspoons	5	milliliters	ml
fluid ounces	fluid ounces	30	milliliters	ml
cup	cup	0.24	liters	l
quarts	quarts	0.95	liters	l
gallons	gallons	3.8	liters	l
cubic feet	cubic feet	0.03	cubic meters	m ³
cubic yards	cubic yards	0.76	cubic meters	m ³
TEMPERATURE (exact)				
°F	Fahrenheit temperature	5/9 (after subtracting 32)	Celsius temperature	°C

*1 in = 2.54 (exact). For other exact conversions and more detailed tables, see NBS Misc. Publ. 286, Units of Length and Masses, Price \$2.25, SD Catalog No. C13.10.286.

Approximate Conversions from Metric Measures

Symbol	When You Know	Multiply by	To Find	Symbol
LENGTH				
mm	millimeters	0.04	inches	in
cm	centimeters	0.4	inches	in
m	meters	3.3	feet	ft
m	meters	1.1	yards	yd
km	kilometers	0.6	miles	mi
AREA				
cm ²	square centimeters	0.16	square inches	in ²
m ²	square meters	1.2	square yards	yd ²
km ²	square kilometers	0.4	square miles	mi ²
ha	hectares (10,000 m ²)	2.5	acres	acres
MASS (weight)				
g	grams	0.035	ounces	oz
kg	kilograms	2.2	pounds	lb
t	tonnes (1000 kg)	1.1	short tons	short tons
VOLUME				
ml	milliliters	0.03	fluid ounces	fl oz
l	liters	2.1	pints	pt
l	liters	1.06	quarts	qt
m ³	cubic meters	0.26	gallons	gal
m ³	cubic meters	35	cubic feet	ft ³
m ³	cubic meters	1.3	cubic yards	yd ³
TEMPERATURE (exact)				
°C	Celsius temperature	9/5 (then add 32)	Fahrenheit temperature	°F

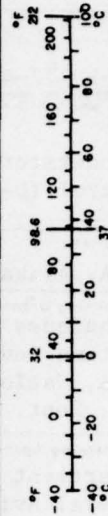


TABLE OF CONTENTS

Abstract

ACCESS	
NIS	on <input checked="" type="checkbox"/>
DD	3 if So Don <input type="checkbox"/>
MA	MA <input type="checkbox"/>
J'S	
BY	
DISTRIBUTION AVAILABILITY CODES	
DI	SPECIAL
<div style="display: flex; justify-content: space-between;"> <div style="width: 30%; text-align: center;">A</div> <div style="width: 35%;"></div> <div style="width: 35%;"></div> </div>	

1. INTRODUCTION

In a previous report (Alaka, et al., 1975), we described preliminary results of a research and development effort to improve aviation weather forecasts performed under Interagency Agreement No. DOT FA74WAI-488 between the Federal Aviation Administration (FAA) and the National Weather Service (NWS). The immediate aim of this effort is to develop improved objective forecasts of local convective weather, particularly thunderstorms, at high density terminals and surrounding airspace. The effort falls within the broad purpose of the agreement, which is to develop, test, and implement improved forecast techniques of aviation weather in the 0-6 hour time range.

The time range and content of aviation forecasts must meet the operational requirements of both enroute and terminal controllers as well as flow controllers and pilots. The center and terminal controllers who are in direct contact with the pilot need sufficient detail to plan for deviation requests and, when possible, to give avoidance advisories to aircraft under their control. They are, therefore, interested in current hazardous conditions and the changes likely to occur in these conditions. Timely forecasts with projections of 10 minutes to 2 hours will best suit the needs of the terminal controller.

Flow controllers, on the other hand, are more concerned with the number of aircraft a given route or terminal can accommodate. Therefore, they need to know the meteorological conditions which will exist in both the enroute and terminal areas. Although most flights are of comparatively short duration, some last several hours. To enable flow controllers to utilize the airspace, most effectively, forecasts of several hours over a comparatively large area are needed. This will enable the controller to anticipate and plan for expected traffic flow adjustments caused by deteriorating weather.

To satisfy the needs of the above two categories of users, we have divided our total effort into two main tasks, the first dealing with "very short" (0-2 hour) forecasts and the second with "short" (2-6 hour) forecasts. This division is convenient since a different approach is best suited for each forecast range.

2. VERY SHORT (0-2 hr) FORECASTS

One of the best practical ways (if not the only way) of determining, with sufficient detail and timeliness, the location, movement, and development of convective weather, hazardous to aviation, is to monitor the associated radar echoes. We therefore decided that observations from WSR-57 radars should constitute our main data base for these very short forecasts. In particular, we have used reflectivities from these radars, which have been digitized into discrete intensity levels, to provide a basis for their quantitative application. The aim is to use these digitized radar observations to develop automated techniques for identifying, tracking, and extrapolating the motion and development of local convective weather.

systems at and around air terminals. Since timeliness is of the essence, we have placed due emphasis on techniques which can be readily implemented with locally available facilities.

In recent years several studies have been made to determine the predictability of radar echo motion. A summary of such studies was given in a preliminary report (Alaka, et al., 1975) and more recently by Elvander (1976). So far, no systematic effort has been made to determine the comparative merit of the different techniques used by different investigators.

2.1 Techniques selected for study

For the purpose of this study we have selected three methods of various degrees of complexity. The first consists of obtaining a displacement vector for the entire PPI. This may be done by either a cross-correlation or error minimization technique. The procedure described by Austin and Bellon (1974) is an example of the cross-correlation method which we shall call the CCM model. In this model, all data above a pre-determined threshold are used in the computations. Individual echoes are not considered. Two successive PPI's are space lagged with respect to one another and correlation coefficients are computed. The technique uses a methodology whereby relatively small amounts of computations are necessary. The correlation subroutine is used twice. The first time only every other row and column of data are used. A rough estimate of the location of the best lags is determined from these computations. The possible lags extend to a maximum of 5 grid lengths in the east-west and north-south directions. During the second time through the correlation subroutine, all the data are used, but only deviations of two grid lengths east-west and north-south are allowed from the lags given by the rough estimate. Ground clutter and data beyond the range of 120 nmi are excluded from the computations.

The second method is to track and extrapolate the motion of echo centroids. This procedure was described by Barclay and Wilk (1970), and Wilk and Gray (1970); we shall refer to it as the LLS method. The LLS technique is almost self-explanatory. Successive positions of echo centroids are used to compute linear x- and y- displacement equations by the method of least squares. The echo centroids are then extrapolated according to the required time interval. Computations are allowed only if three or more past centroid positions are available. The entire echo is moved according to the nearest whole grid length. Forecasts of echo centroid positions are verified by observations, and the resulting statistics assembled. These data are all in standard decimal form. However, it is the area of coverage of echoes of a given intensity that is verified in these experiments.

The third method tracks individual echoes by first considering the entire echo complex and then making adjustments for

individual echoes defined in accordance with certain criteria. This method was developed at the Stanford Research Institute (SRI) under contract with the National Weather Service and was described by Duda and Blackmer (1972) and Blackmer, Duda and Reboh (1973). We shall refer to it as the SRI model.

The SRI model isolates, tracks, and forecasts the motion of individual echoes. A contouring technique is used to isolate these echoes. Data in a given row are scanned forward and backward, and grid points with an intensity below a pre-determined threshold are set to zero. Then rows immediately above and below are similarly scanned. Directed line segments from one zero value to another constitute a boundary. However, isolated zero values which are surrounded by non-zero values are not considered in delineating the boundary. An echo is defined as the area within the boundary. The extreme rows and columns where non-zero values are located form a rectangular "window" surrounding the echo. This window is subsequently used in the tracking program. Pertinent statistics are computed for each echo identified by this procedure. These include the significance weight, echo size, center of mass, center of echo area, maximum intensity, and average intensity.

The tracking program consists of matching successive radarscopes (PPI's) by a cross-correlation technique which involves minimizing the sum of the absolute differences between the intensity digits over the entire radarscope (global matching) or over selected windows (local matching). This is done by moving one radarscope relative to the other until the best match is obtained.

To initiate the tracking procedure, significant echoes are identified on the first PPI and the remaining digits are set to zero. A global match is then made between the filtered first PPI and the next PPI. The displacement thus obtained is applied to each significant window in the first PPI and is modified by local matching. The displacement obtained from both global and local matches is then used as the actual displacement of the echo. Predicted displacements for the next echo are a weighted average of the previous predicted and latest actual displacements. This allows past history of the echo motion to be incorporated in the forecast.

Four situations may occur when two successive PPI's are matched: the significant echoes may remain essentially unchanged, become lost, split, or merge. If they split, the largest fragment is retained as the old echo. If they merge, a check is made to ensure that each new echo is different from all other echoes. Lost echoes may later

be recovered. Pertinent statistics are computed for the successfully matched echoes which are then removed from the PPI.

The PPI is then scanned for significant new echoes. Often a new echo appears to be in the path of an echo lost during an earlier PPI processing. A check is made to make sure that this is indeed the case. Pairings are then made between the old lost echoes and the new echoes according to certain criteria which tend to minimize the number of spurious new echoes and lead to more consistent tracks.

If a new echo is obtained without any previous history, it is assigned a predicted displacement that is a function of the surrounding echoes. Those echoes which are closest and with the largest tracking histories are given the highest weight.

The displacements used to make forecasts are slightly different from those used in the tracking portion of the model. They are also a weighted average of the previously predicted displacement and the last actual displacement. But now, echoes with a long tracking history have a higher weight than those with a short lifespan. The entire echo, isolated during the last PPI used, is moved during the forecast interval. The area predicted to be covered by echoes of predetermined intensities is verified in these experiments.

We have adapted versions of the above three methods to test their comparative performance. We have somewhat relaxed the original SRI echo definition criteria. Thus in defining an echo of a given intensity threshold, we allow an intensity value of one digit less than the threshold to exist between two consecutive higher values, both in the orthogonal and diagonal directions.

2.2 Data used in the study

We have used digitized weather radar data originally collected and archived at the National Severe Storms Laboratory (NSSL) during the spring season of 1972. The original data are in the form of nine intensity digits representing the power in dbm returned by the target. The data were collected by NSSL's WSR-57 weather radar at Norman, Oklahoma, over a range extending from 14 to 125 nmi, on a polar grid of 1 nmi radial distance and 2 deg azimuth. We have transferred these data by quadratic interpolation to a cartesian grid of 120 x 120 points, 2 nmi apart. We have also represented the data on a coarser 60 x 60 grid of squares 4 nmi on a side, attributing to each square the maximum reflectivity value observed over the 16 nmi² area.

We have used the available reflectivities observed at different elevation angles to compute values of the vertically integrated liquid water (VIL) content. As in the case of zero degree reflectivities mentioned above, we have represented the VIL data on a 120 x 120 grid and a 60 x 60 grid. The value attributed to each 16 nmi² square in the coarser grid is the maximum value found in the corresponding four 4 nmi² squares of the finer grid.

We have tested the three methods described above on five storm days from the NSSL spring 1972 data set. These are April 13, 19, 20, 26, and May 22-23. These days which had varying types of convective weather, severe on occasion, are representative of conditions to be expected in real-time operations. No stratiform rain type situations are included in this study.

2.3 Verification Procedures

As mentioned above, different methods of forecasting radar echo motion have not previously been evaluated according to the same criteria, thus leading to difficulties in attempting to assess their comparative merit. In the present study, we have subjected all three methods selected for testing, to the same verification scores. Table 1 provides the basis for computing the scores. A successful forecast (X) is scored when both predicted and observed values of radar reflectivities or VIL are equal to or larger than the predetermined threshold. A miss (Y) occurs when a value equal to or larger than the predetermined threshold is observed but not forecast. A false alarm (Z) occurs when a value equal to or larger than the predetermined threshold is forecast but not observed. Cases involving correct forecasts of subthreshold values (W) are not included in the verification statistics.

Table 1. Contingency table defining the variables used in computing the verification scores.

Observed	Forecast	
	Value equal to or larger than threshold	Value less than Threshold
Value equal to or larger than threshold	X	Y
Value less than threshold	Z	W

Following are the scores used and their definitions:

- a. Probability of Detection (POD) described by Donaldson et al., (1975), also referred to by Panofsky and Brier (1958) as "prefigurance."

$$\text{POD} = X \div (X + Y) \quad (1)$$

- b. False Alarm Ratio (FAR), (Donaldson et al., 1975).

$$\text{FAR} = Z \div (X + Z) \quad (2)$$

- c. Critical Success Index (CSI), (Donaldson, 1975), commonly known as the "threat score," (Palmer and Allen, 1949).

$$\text{CSI} = X \div (X + Y + Z) \quad (3)$$

We verified our forecasts over areas of 16 and 64 nmi². The 16 nmi² area is very close to that of a grid-box in the D/RADEX system (Bigler, et al., 1973; Saffie, 1976). The 64 nmi² area is about the size of the Washington, D.C. metropolitan area. This area would cover the approaches to most airports as well as the terminal itself. An idea of the numbers involved in computing the verification scores is illustrated by Table 2 which lists the total number of forecasts (X + Y + Z in Table 1) by the SRI model for different threshold intensities, data sequences, forecast projections, and verification areas.

Table 2. Total number of forecasts made by the SRI model from zero tilt reflectivity data, verified over 16 nmi² and 64 nmi², and from VIL data, verified over 16 nmi².

Reflectivity threshold	10-min Data			30-min Data		
	Forecast Projection (minutes)			Forecast Projection (minutes)		
	10	30	60	30	60	90
<u>16 nmi² Verification Area</u>						
1	81373	86486	86390	31287	30102	27841
2	55096	58603	58510	20470	19968	19033
3	40334	43382	42848	14839	14888	14132
4	24681	27068	27112	8694	8771	8434
<u>64 nmi² Verification Area</u>						
1	123503	130626	131121	46319	45510	29170
2	90807	95728	95763	32047	31638	30148
3	68941	73498	72496	24565	24842	23722
4	44159	47778	48493	15389	15688	15328
<u>VIL threshold</u>						
<u>16 nmi² Verification Area</u>						
1	15561	22158	21752			
2	6412	6548	5430			
3	4393	4527	3849			
4	3220	3407	3018			
5	2657	2884	2451			

2.4 Results

We have tested the three forecast models using both 10- and 30-minute sequences of input data. We used the SRI and LLS model to produce 10-, 30-, and 60-minute forecasts from 10-minute data sequences, and 30-, 60-, and 90-minute forecasts from 30-minute sequences. With the CCM model, we made forecasts of 10-, 30-, and 60-minutes from 10-minute data sequences, and 30- and 60-minute forecasts from 30-minute sequences.

The SRI model uses two criteria to identify echoes for tracking purposes--a reflectivity threshold and a significance weight (SW) threshold. The formula for the latter is:

$$S.W. = 100 \log_{10} \left[\left(\frac{Z_{\max}}{Z_{\text{ref}}} \right)^{0.5} \left(\frac{\sum Z^{1/1.6}}{Z_{\text{ref}}^{1/1.6}} \right) \right] \quad (4)$$

where Z_{ref} is an arbitrary normalization reflectivity value of $100 \text{ mm}^6/\text{m}^3$, Z_{\max} is the reflectivity corresponding to the highest intensity integer, and $Z^{1/1.6}$ is the Marshall-Palmer rainfall-rate estimate (1948). Thus, the first term of the significance weight accounts for the maximum reflectivity within the cell, while the second term, which is a sum of Z values meeting a predetermined intensity threshold, is a measure of echo size. Both factors are known to be pertinent to the severity of convective weather. The SRI significance weight thus imposes a selectivity constraint on the data because only echoes which are either intense or large, or both, are considered significant enough for tracking. As an illustration, Figure 1 gives different echo configurations having a significance weight of 150. The trade-off between maximum intensity within the cell and the size of the cell is clearly indicated. Small intense cells are selected as well as larger less intense cells. For an intensity threshold of 3 and significance weight of 150, an isolated value of intensity 5 or 6 will qualify the echo for tracking. In comparison, an echo intensity level 3 must extend over 9 grid boxes to be selected for tracking.

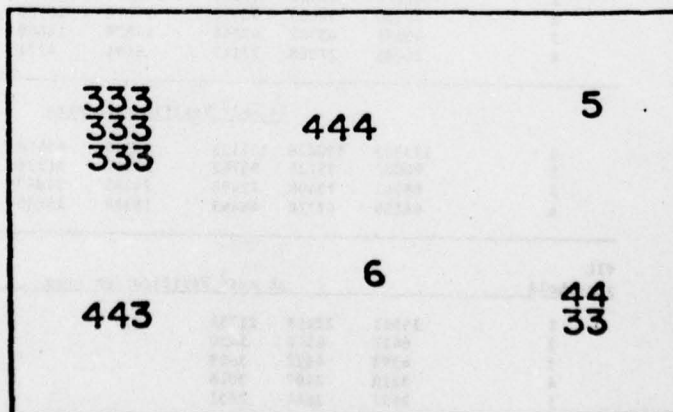


Figure 1. Different configurations of zero-degree reflectivities having an intensity threshold of 3 and an SRI significance weight threshold of 150.

The CCM model uses only a reflectivity threshold, and is thus less selective.

In most of our experiments with the SRI and LLS models, we have used the following combinations of reflectivity thresholds and significance weights: (1,25), (2,50), (3,150) and (4,200). We also made several runs with these models using only a reflectivity threshold to make the results more strictly comparable with those from the CCM model. Surprisingly, results were very similar.

Tables 3-5 list the results of our tests on zero degree reflectivities over a predictand area of 16 nmi^2 . Table 3, relating to the probability of detection (POD) shows that the cross-correlation (CCM) technique is superior to the others on this score. The SRI method fares worst in general. The CCM technique also has the highest critical success index (CSI) except when 30-minute forecasts are made from 10-minute data sequences (Table 4). The SRI method scores somewhat higher for such forecasts. The linear least-square extrapolation (LLS) technique shows the worst CSI scores. The SRI method redeems itself by its low false alarm ratio (FAR), particularly for the 30- and 60-minute forecasts from 10-minute data sequences (Table 5). However, this advantage disappears when 30-minute data sequences are used.

When a 64 nmi^2 predictand area is used, the CCM is best in POD (Table 6), it also has the highest CSI scores for forecasts from both 10-minute and 30-minute data sequences (Table 7). Its FAR score lags behind that of the SRI model for forecasts made from 10-minute data input (Table 8). The LLS technique is again generally outranked by the other techniques on all scores.

Results are somewhat different when vertically-integrated liquid-water (VIL) content data are used (Tables 9-11). We tested only 10-minute input data sequences. When all the VIL data are used in the computations, the CCM model is still the best performer. However, when only high VIL values are considered, the LLS model scores are the highest.

We conclude that if we are interested in 60-minute high resolution forecasts of reflectivity patterns and have 10-minute data sequences, it may be advantageous to use the SRI technique especially if we wish to keep the number of false alarms relatively low. However, this would require a relatively large computer capability and the forecasts may have to be performed in a central computer facility. If, on the other hand, we prefer a relatively simple technique which may be implemented locally on a mini-computer, the CCM method recommends itself, especially for low-resolution forecasts of 30-minutes or less. For tracking VIL patterns, an LLS type model, using only the more intensive values, is recommended.

Table 3. Values of the cumulative Probability of Detection for forecasts made by the three models from all five test days, verified over a 16 nmi² grid box area.

Zero Tilt Reflectivity Data		POD (10-min input)			POD (30-min input)		
Model - Integer Threshold		Forecast Length			Forecast Length		
		10	30	60	10	30	60
CCM	1	78	62	49	62	53	--
	2	74	55	43	53	47	--
	3	72	51	37	53	42	--
	4	67	42	28	46	33	--
LLS	1	60	37	24	50	35	27
	2	60	42	26	40	27	19
	3	57	35	23	31	19	14
	4	54	32	19	30	16	11
SRI	1	75	42	28	36	19	12
	2	68	37	23	41	29	21
	3	63	32	20	31	18	12
	4	60	28	16	29	16	11

Table 4. Values of the cumulative Critical Success Index for forecasts made by the three models from all five test days, verified over a 16 nmi² grid box area.

Zero Tilt Reflectivity Data		CSI (10-min input)			CSI (30-min input)		
Model - Integer Threshold		Forecast Length			Forecast Length		
		10	30	60	10	30	60
CCM	1	62	42	28	41	31	--
	2	58	36	24	33	26	--
	3	55	32	20	33	23	--
	4	50	26	15	28	17	--
LLS	1	46	26	17	35	23	17
	2	47	31	18	28	18	12
	3	44	25	16	21	12	8
	4	41	22	12	20	10	6
SRI	1	62	42	27	24	13	8
	2	57	37	23	30	21	15
	3	53	32	20	22	13	8
	4	49	28	16	21	11	7

Table 5. Values of the cumulative False Alarm Ratio for forecasts made by the three models from all five test days, verified over a 16 nmi² grid box area.

Zero Tilt Reflectivity Data		FAR (10-min input)			FAR (30-min input)		
Model - Integer Threshold		Forecast Length			Forecast Length		
		10	30	60	10	30	60
CCM	.1	24	44	60	45	58	--
	2	27	50	65	53	63	--
	3	30	54	69	53	67	--
	4	33	60	76	59	73	--
LLS	1	34	52	63	45	49	67
	2	31	48	61	52	65	75
	3	33	54	66	60	75	82
	4	36	59	72	63	81	89
SRI	1	21	34	48	57	71	77
	2	21	38	52	47	57	64
	3	24	43	57	56	71	78
	4	27	49	66	58	74	82

Table 6. Values of the cumulative Probability of Detection for forecasts made by the three models from all five test days, verified over a 64 nmi² grid box area.

Zero Tilt Reflectivity Data		POD (10-min input)			POD (30-min input)		
Model - Integer Threshold		Forecast Length			Forecast Length		
		10	30	60	10	30	60
CCM	.1	83	69	57	69	60	--
	2	80	65	52	64	55	--
	3	77	61	47	61	50	--
	4	75	53	38	59	43	--
LLS	1	80	53	36	59	44	34
	2	70	49	36	48	35	25
	3	64	43	30	39	27	20
	4	60	40	27	39	24	17
SRI	1	75	49	34	45	26	12
	2	68	43	29	47	34	26
	3	61	37	25	37	40	17
	4	58	34	20	35	22	15

Table 7. Values of the cumulative Critical Success Index for forecasts made by the three models from all five test days, verified over a 64 nmi² grid box area.

Zero Tilt Reflectivity Data		CSI (10-min input)			CSI (30-min input)		
Model - Integer Threshold		Forecast Length 10 30 60			Forecast Length 10 30 60		
CCM	1	69	50	35	49	37	--
	2	65	46	31	44	33	--
	3	62	41	27	40	29	--
	4	59	36	22	39	24	--
LLS	1	62	37	25	44	30	23
	2	59	42	26	40	24	17
	3	52	35	22	31	18	13
	4	49	32	19	30	15	10
SRI	1	69	49	34	32	18	12
	2	62	43	28	36	26	26
	3	56	37	25	28	18	17
	4	53	34	20	27	16	15

Table 8. Values of the cumulative False Alarm Ratio for forecasts made by the three models from all five test days, verified over a 64 nmi² grid box area.

Zero Tilt Reflectivity Data		FAR (10-min input)			FAR (30-min input)		
Model - Integer Threshold		Forecast Length 10 30 60			Forecast Length 10 30 60		
CCM	1	20	36	52	37	50	--
	2	27	40	56	41	55	--
	3	30	44	60	45	59	--
	4	33	49	66	47	64	--
LLS	1	22	40	54	36	50	58
	2	20	38	51	41	55	65
	3	22	41	55	47	64	73
	4	24	45	60	50	71	81
SRI	1	16	29	41	47	63	77
	2	16	30	43	39	49	55
	3	17	34	46	46	61	69
	4	19	38	55	45	62	72

Table 9. Values of the cumulative Probability of Detection for forecasts made by the three models from all five test days, verified over a 16 nmi² grid box area.

VIL Data		POD (10-min input)		
Model - Integer Threshold		Forecast Length		
		10	30	60
CCM	1	73	58	47
	2	69	49	36
	3	66	44	30
	4	64	43	28
	5	62	42	28
LLS	1	74	79	60
	2	66	45	30
	3	65	40	27
	4	61	42	25
	5	61	40	21
SRI	1	83	75	66
	2	69	47	31
	3	63	38	23
	4	56	33	12
	5	49	24	9

Table 10. Values of the cumulative Critical Success Index for forecasts made by the three models from all five test days, verified over a 16 nmi² grid box area.

VIL Data		CSI (10-min input)		
Model - Integer Threshold		Forecast Length		
		10	30	60
CCM	1	57	37	25
	2	52	30	18
	3	50	26	15
	4	47	25	14
	5	46	25	14
LLS	1	25	19	15
	2	49	29	19
	3	49	26	17
	4	49	30	17
	5	49	27	13
SRI	1	46	27	18
	2	52	31	20
	3	47	25	15
	4	44	22	9
	5	37	15	5

Table 11. Values of the cumulative False Alarm Ratio for forecasts made by the three models from all five test days, verified over a 16 nmi² grid box area.

VIL Data		FAR (10-min input)		
Model - Integer Threshold		Forecast Length		
		10	30	60
CCM	1	27	49	65
	2	31	58	72
	3	33	61	76
	4	36	62	78
	5	37	63	77
LLS	1	73	69	83
	2	35	56	67
	3	34	57	67
	4	29	51	67
	5	30	54	74
SRI	1	49	71	80
	2	32	53	64
	3	34	57	71
	4	34	60	81
	5	40	71	88

2.5 Future Plans

We are concentrating our future effort on two main tasks--determining the relationship between severe weather events and parameters derived from digital weather radar, and developing a short range forecast of the probability of echoes of a predetermined intensity occurring at each grid box over the radarscope area.

Archived digital radar data will be used to develop cartesian maps of zero tilt reflectivity and VIL data. Cells will be defined objectively from these data. Parameters will be defined for each cell and these parameters will be related statistically to the occurrence of severe weather in the cell. An operational mode would entail defining the cells objectively, computing the necessary parameters for each cell, and applying the correct equation to determine the probability of severe weather associated with that cell.

Similarly we shall use archived D/RADEX data to forecast the probability of occurrence of radar echoes of predetermined intensities using, as predictors, forecasts of echo movements by appropriate tracking models, and previous radar observations, and trends. Other potential predictors to be considered are VIL data, echo tops, tropopause penetration, and various synoptic meteorological and satellite data. Eventual implementation will result in maps of forecast probabilities of echoes of predetermined intensity over the entire grid. These should prove applicable for Air Traffic Control.

3. SHORT RANGE (2-6 hr) FORECASTS

As mentioned earlier, this task was initiated to satisfy the needs of flow controllers who need forecasts of several hours over a comparatively large area to enable them to divert air traffic threatened by inclement weather to safe terminals.

In our interim report (Alaka, et al., 1975) we discussed a preliminary prediction scheme which showed a good deal of promise. We have since expanded and improved the developmental procedure. We have in effect: (1) added new predictors derived from new data sources, (2) increased the size of the developmental data sample, and (3) expanded the geographical domain of the forecasts.

We are now transmitting to the field, three times daily, computer produced 2-6 hr probabilities of thunderstorms. The forecasts span the period 1700-0300 GMT, which is the period of maximum diurnal frequency of thunderstorms.

3.1 Development of prediction equations

Our prediction scheme continues to be based on a combination of classical statistical (Klein, 1970) and model output statistics (MOS) approaches (Glahn and Lowry, 1972). We have derived separate prediction equations for each of the periods 1700-2100, 2000-0000, and 2300-0300 GMT. The developmental data sample was derived from the spring season (mid-March to mid-June) of 1974 and 1975. Because of the smallness of this sample, we used the generalized operator approach over the entire area delineated in Figure 2.

3.1.1 Thunderstorm predictands

In developing our statistical sample, we have determined thunderstorm occurrence from manually digitized radar (MDR) data. Radar echo intensities and coverage are digitized over square areas 40-45 nmi on a side in accordance with ten-digit code from 0-9 (Moore, Cummings, and Smith, 1974). A thunderstorm is assumed to occur within an MDR square whenever the MDR code for that square equals or exceeds 4 during the 4-hr forecast periods mentioned above. This assumption is reasonable in view of the results obtained by Mogil (1974) and Reap and Foster (1975). Altogether, there are 571 MDR squares over the predictand area depicted in Figure 2. The predictand is assigned a value of 1 for a thunderstorm occurrence and 0 otherwise.

3.1.2 Thunderstorm predictors

Potential predictors were developed from four data sources, namely, basic hourly surface meteorological observations, forecasts of basic upper air variables by the Limited-area Fine Mesh model (LFM) of NMC

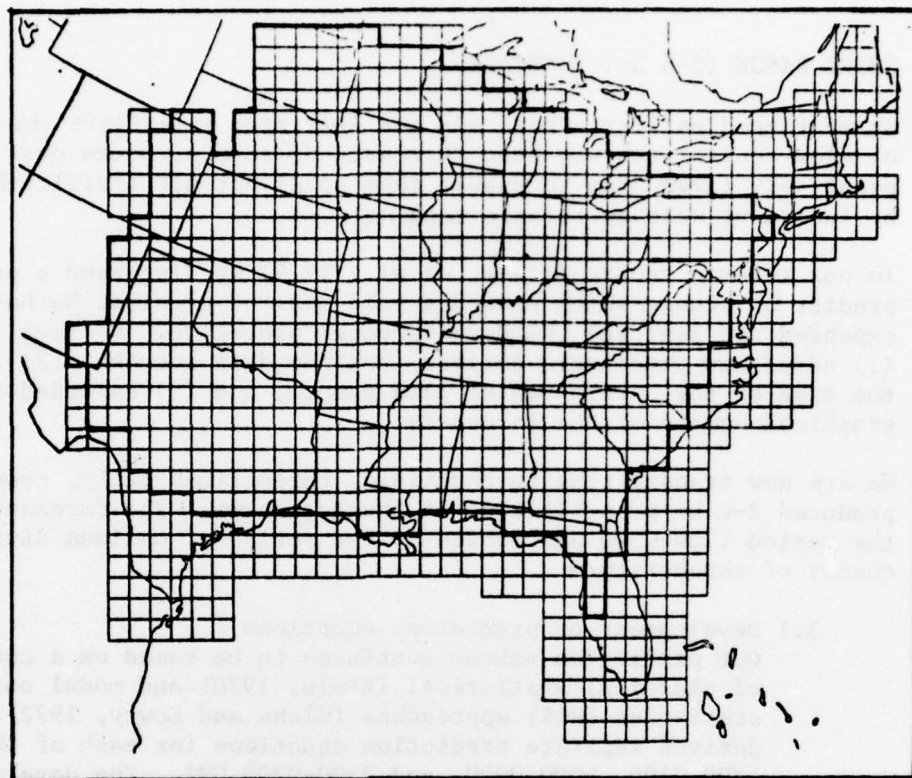


Fig. 2. The general thunderstorm predictands were defined within that region of the U. S. enclosed by the heavy line. The individual predictand boxes correspond to the MDR squares shown; predictors are evaluated at the centers of these boxes.

(Howcroft and Desmarais, 1971), MDR reports, and the climatological relative frequency of the predictand.

The valid times of the various data sources relative to the forecast period are shown in Figure 3. Thus the MDR observations are 2 1/2 hr earlier than the

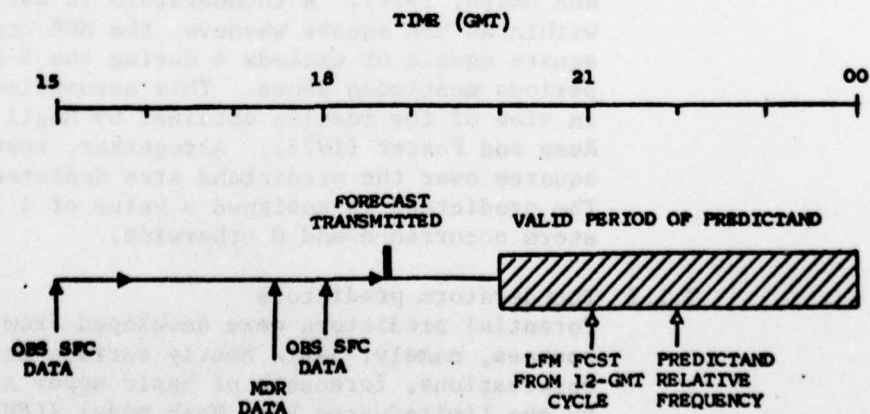


Fig. 3. Types of input data and their valid times relative to the valid period of the predictand for the 1800-GMT forecast cycle.

beginning of the forecast period, the observed surface data are 5 and 2 hr earlier, and the LFM forecasts are valid 1 hr afterwards. The potential predictors are evaluated at the centers of the predictand boxes. Therefore the surface observations and LFM forecasts had to be interpolated to these points. In the case of the surface observations, this was done by analyzing the data in accordance with a successive approximation scheme (Cressman, 1959). LFM forecasts were evaluated by standard interpolation from the LFM grid to the centers of MDR boxes.

The potential predictors are listed in Table 12 which also shows the data sources from which they were obtained. The list is mostly self-explanatory, but the following instability indices, well-known for their pertinence to thunderstorm prediction, require definition:

- a. The K-index (George, 1960)

$$K = (T + T_d)_{850} - (T - T_d)_{700} - T_{500} \quad (5)$$

where T denotes the temperature, T_d the dew-point and the suffixes indicate the level.

- b. The modified K-index, K', where

$$K' = \frac{1}{2} (T_{sfc} + T_{850} + T_{d_{sfc}} + T_{d_{850}}) - (T - T_d)_{700} - T_{500} \quad (6)$$

- c. The Total Totals (TT) index (Miller, 1972) where

$$TT = (T + T_d)_{850} - 2T_{500} \quad (7)$$

- d. The modified Total Totals (TT)'

$$TT' = \frac{1}{2} (T_{sfc} + T_{850} + T_{d_{sfc}} + T_{d_{850}}) - 2T_{500} \quad (8)$$

- e. The Showalter index (SI) (Showalter, 1953)

$$SI = T_{500} - T^* \quad (9)$$

where T* is the predicted temperature of an air parcel lifted dry adiabatically from 850 mb to saturation, then moist adiabatically to 500 mb.

f. The modified Showalter index

$$SI' = T_{500} - T^* \quad (10)$$

where T^* is the observed temperature of an air parcel lifted dry adiabatically from the surface to its saturation, then moist adiabatically to 500 mb.

Table 12. Potential thunderstorm predictor variables. The data source(s) for each variable is given in the right hand column.

Variable	Data Source(s)
1. Sfc u-component	Sfc obs
2. Sfc v-component	Sfc obs
3. BL u-component	LFM
4. BL v-component	LFM
5. 850-mb u-component	LFM
6. 850-mb v-component	LFM
7. 500-mb u-component	LFM
8. 500-mb v-component	LFM
9. MSL pressure	Sfc obs
10. 700-mb vertical velocity	LFM
11. Sfc mixing ratio	Sfc obs
12. 850-mb mixing ratio	LFM
13. 700-mb mixing ratio	LFM
14. 850- to 500-mb mean mixing ratio	LFM
15. 850- to 500-mb mean temp.-dew point	LFM
16. Sfc equiv. pot. temp.	Sfc obs
17. Sfc equiv. pot. temp. x horizontal gradient of sfc equiv. pot. temp.	Sfc obs
18. 850-mb equiv. pot. temp.	LFM
19. 700-mb equiv. pot. temp.	LFM
20. 850- to 700-mb mean equiv. pot. temp.	LFM
21. (Sfc minus 700 mb) equiv. pot. temp.	Sfc obs + LFM
22. (850 mb minus 700 mb) equiv. pot. temp.	LFM
23. Sfc equiv. pot. temp. advection	Sfc obs
24. 850-mb equiv. pot. temp. advection	LFM
25. 700-mb equiv. pot. temp. advection	LFM
26. Sfc moisture divergence	Sfc obs
27. BL moisture divergence	Sfc obs + LFM
28. 850-mb moisture divergence	LFM
29. K index	LFM
30. Modified K index	Sfc obs + LFM
31. Total Totals index	LFM
32. Modified Total Totals index	Sfc obs + LFM
33. Showalter index	LFM
34. Modified Showalter index	Sfc obs + LFM
35. 500-mb wind speed	LFM
36. Mag. of 850- to 500-mb wind shear	LFM
37. Signed mag. of 850- to 500-mb 500-mb wind shear	LFM
38. (500 mb minus 850 mb) wind direction.	LFM
39. BL vorticity	LFM
40. 500-mb vorticity	LFM
41. 500-mb vorticity advection	LFM
42. Three-hr MSL pressure change	Sfc obs
43. MDK variables (see Fig. 5)	MDK data
44. Predictand relative frequency	Predictand data

Each of the variables computed in Table 12 was smoothed to remove wavelengths of 4 grid-lengths and less. A five-point hanning filter (Shuman, 1957) was used.

3.1.3 Optimum predictor locations

Thunderstorms occur on a scale considerably smaller than that which the regularly available conventional observations and numerical forecasts can resolve. An ex-

ception is the weather radar which is capable of depicting smaller scale features associated with these phenomena. Unfortunately, current operational radar information is largely qualitative, and the manual digitization of radar reflectivities is an attempt to quantize this information. The MDR data we are using provide, in effect, the only predictor input which is even remotely comparable in scale to the predictand.

Our task, then, is to predict the small-scale thunderstorms from data which are essentially large (synoptic) scale. It is a common experience by those familiar with synoptic maps that the meteorological fields depicted by these maps form recognizable patterns of pressure, wind, temperature, and humidity or of other parameters derived from them. It is also a common experience that these patterns, singly or in combination, are precursors or concomitants of different weather phenomena. However, neither do the salient characteristics of these patterns necessarily coincide with one another in time and space, nor do they usually coincide with the location of the weather with which they are associated. As an example, while it is known that low pressure is associated with rainy weather, it does not follow that the rainiest weather occurs where the pressure is lowest. Thus, a most effective use of the predictors in Table 12 is not compatible with the assumption that the predictors are collocated with the predictand. An effort must therefore be made to determine the optimum location of the different potential predictors relative to that of the predictand. This is especially important in the present case since most of our predictors are based on observations made several hours before predictand time.

We have devised a scheme to determine the optimum position of each potential predictor. We defined the best position as that which yields the highest linear correlation with the predictand from among 30 points surrounding the predictand box. The best positions relative to a predictand box of 10 potential predictors are illustrated in Figure 4.

Because fields of radar echoes are highly discontinuous, we decided to offer, as potential predictors, MDR values for a relatively large number of boxes surrounding the predictand box. To determine which MDR boxes were most useful, we ran a special screening regression in which 30 candidate boxes were offered. The first 7 boxes selected (Fig. 5) were chosen as the potential predictors to be used in combination with the other variables in Table 12.

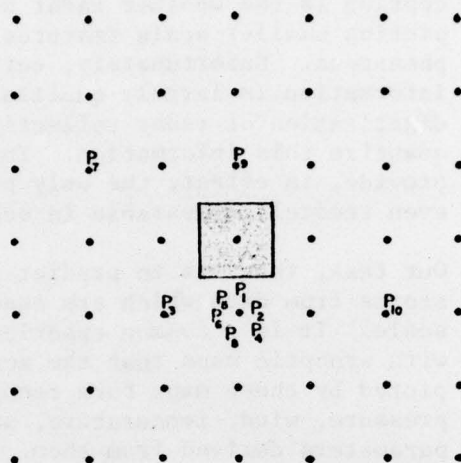


Figure 4--The P's denote grid point positions of different predictor variables relative to the predictand box. The position of each variable was determined from the field of space-lagged linear correlation coefficients where the correlation is between that variable and the predictand; the highest correlation specified the position or offset of the variable relative to the predictand box (shaded). The subscripts to the P's are in the order of decreasing magnitude of the linear correlation coefficients. Each variable is identified below; the trailing information in parentheses gives the sign of the correlation coefficient and the data from which the variable was computed:

- P₁ - Modified K index (+; Sfc obs + LFM)
- P₂ - Showalter index (-; LFM)
- P₃ - Modified Total Totals index (+; Sfc obs + LFM)
- P₄ - 850-mb mixing ratio (+; LFM)
- P₅ - 850- to 500-mb mean mixing ratio (+; LFM)
- P₆ - Sfc moisture divergence (-; Sfc data)
- P₇ - Equiv. pot. temp. x horizontal gradient of equiv. pot. temp (+; Sfc data)
- P₈ - Sfc equiv. pot. temp. advection (+; Sfc data)
- P₉ - 500- mb v-component (+; LFM)
- P₁₀ - 500-mb wind speed (-; LFM)

3.1.4 Linearizing predictor-predictand relationships

The screening regression technique, used to derive the prediction equations, relates the predictand to a weighted linear combination of the predictor variables. However, in general the predictor-predictand relationships are in fact non-linear, except within limited ranges, or in segments (Alaka, et. al., 1973). To deal with this problem, predictors are usually either truncated to exclude the range where their relationships with predictand frequency are highly non-linear, or their total range is divided into short segments with each segment being treated as a binary predictor (Miller, 1964). The drawbacks of this procedure are: (1) lack of a priori guidance in defining the binary limits, (2) the total number of predictors can

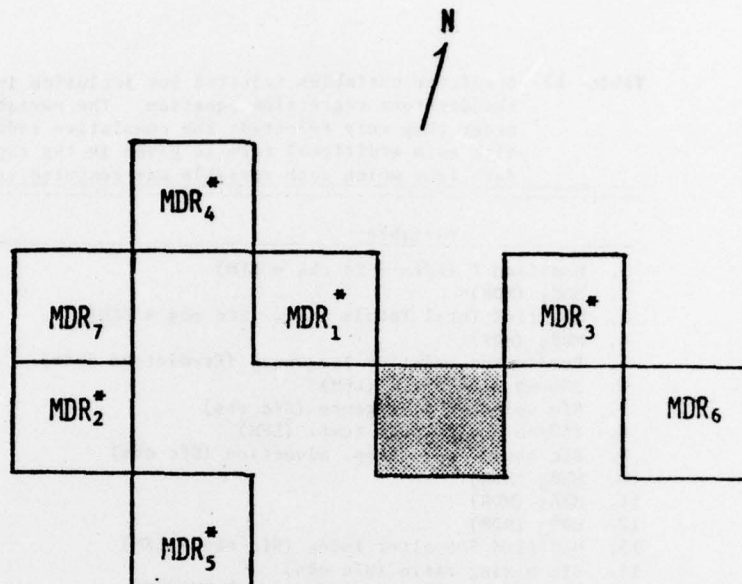


Fig. 5. Potential predictors defined from MDR data. The subscripts denote the order of selection of seven MDR predictor boxes in a special screening regression run wherein 30 MDR boxes surrounding the predictand box were offered. The predictor boxes selected for inclusion into the 1800 GMT equation are indicated by asterisks. The predictand box is indicated by shading.

become exceedingly large, and (3) there is no assurance that the predictive information of the predictor over its entire range is completely utilized.

Our procedure to deal with the non-linearity between each predictor and predictand involved computing the predictand frequency for short intervals over the range of the potential predictor values (Charba, 1977a). The predictand frequency for each value of the predictor was subsequently obtained by linear interpolation between computed values. Among the predictors in Table 12 those derived from surface observations and from LFM output were linearized in this manner. A possible disadvantage of this technique may be in "overfitting" the dependent sample, which is especially dangerous when the sample is short.

3.2 Thunderstorm probabilities

We developed two separate thunderstorm probability equations for each predictand period. In the first, the "primary" equation, all the variables in Table 12 were offered for screening as potential predictors. Those selected for the 1800 GMT equation are shown in Table 13 in the order of their selection. This table also shows the data sources for each predictor and the cumulative reduction of variance with each added predictor. It is noteworthy that the cumulative reduction

Table 13--Predictor variables selected for inclusion in the 1800 GMT primary thunderstorm regression equation. The variables are listed in the order they were selected; the cumulative reduction of variance with each additional term is given in the right hand column. The data from which each variable was computed is shown in parenthesis.

Variable	Cumulative Reduction of Variance (%)
1. Modified K index (Sfc obs + LFM)	18.7
2. MDR ₁ (MDR)	20.9
3. Modified Total Totals index (Sfc obs + LFM)	22.3
4. MDR ₂ (MDR)	23.6
5. Predictand relative frequency (Predictand data)	24.2
6. 500-mb wind speed (LFM)	24.9
7. Sfc moisture divergence (Sfc obs)	25.5
8. 850-mb equiv. pot. temp. (LFM)	25.9
9. Sfc equiv. pot. temp. advection (Sfc obs)	26.3
10. MDR ₅ (MDR)	26.6
11. MDR ₄ (MDR)	26.9
12. MDR ₃ (MDR)	27.2
13. Modified Showalter index (Sfc obs + LFM)	27.4
14. Sfc mixing ratio (Sfc obs)	27.7
15. Sfc equiv. pot. temp. (Sfc obs)	28.0
16. 500-mb v-component (LFM)	28.2

of variance increased appreciably out to 16 terms (see Charba, 1977a). Also noteworthy is that all except three of these predictors involve surface observations or MDR data.

The second probability equation, the "backup" equation, was developed without the MDR predictors. The backup equations are used operationally to produce forecasts at grid points where MDR data are missing or unavailable. Table 14 lists the predictors in the order of their selection. Note the considerable rearrangement of the

Table 14--Same as Table 13 for the 1800 GMT "backup" thunderstorm regression equation.

Variable	Cumulative Reduction of Variance (%)
1. Modified K index (Sfc obs + LFM)	18.5
2. Sfc moisture divergence (Sfc obs)	19.8
3. Predictand relative frequency (Predictand data)	20.6
4. Modified Total Totals index--binary (Sfc obs + LFM)	21.3
5. 500-mb wind speed (LFM)	22.0
6. Sfc equiv. pot. temp. advection (Sfc obs)	22.4
7. 850- to 500-mb mean mixing ratio (LFM)	22.8
8. 500-mb v-component--binary (LFM)	23.1
9. Showalter index (LFM)	23.4
10. 850-mb mixing ratio (LFM)	23.6
11. Sfc equiv. pot. temp. x horizontal gradient of equiv. pot. temp. (Sfc obs)	23.8
12. Modified Total Totals index--binary (Sfc obs + LFM)	24.0
13. 850-mb equiv. pot. temp.	24.1
14. Sfc mixing ratio--binary (Sfc obs)	24.3
15. Modified Showalter index (Sfc obs + LFM)	24.5

non-MDR predictors and the selection of some predictors in binary form. As in the primary equation, observed surface data (including predictand frequency) have the greatest input to the equation.

Analogous probability equations were also developed for 1500 and 2100 GMT. Their total reduction of variance and predictand frequency, together with those for 1800 GMT are given in Table 15.

Table 15. Reduction of variance and predictand frequency associated with the primary thunderstorm equation for each of the three times.

Predictor Time (GMT)	Reduction of Variance (%)	Predictand Frequency (%)
1500	24.0	8.4
1800	28.2	10.1
2100	25.8	8.6

3.2.1 Forecast verification

We verified the 1800 GMT forecasts for 2000-0000 GMT transmitted operationally during the spring season of 1976. The 1500 and 2100 GMT forecasts were not verified since there was little reason to believe that results for these times would be substantially different. We tested the forecasts for their bias and for their skill relative to both climatology and persistence.

We defined the bias as the sum of all forecast probabilities divided by the sum of the observations. Unbiased forecasts would therefore have a value of one. The score used to evaluate the skill of the probabilities is based upon a quantity which is one-half the score defined by Brier (1950). This quantity, P , is,

$$P = \frac{1}{N} \sum_{i=1}^N (F_i - O_i)^2 \quad (10)$$

where F_i is the probability estimate and O_i is the observed event for case i . If P_F and P_C are the P -values of the probability and climatic frequency forecasts, respectively, then the skill score, SS , is defined as:

$$SS = \frac{P_C - P_F}{P_C} \times 100. \quad (11)$$

Thus, SS is the percentage of improvement in P of the probabilities over that of climatic frequency forecasts. A positive score would mean that the probabilities are superior to climatology, a negative score would mean the opposite.

The best climatological frequency available for this verification was the predictand relative frequency for individual grid boxes computed from the dependent sample. Since this quantity was also selected as a predictor, the skill score actually measures the forecasting skill of the other predictors.

The independent sample from which the verification statistics were compiled, ran from 31 March to 14 June 1976. With probabilities at all 571 forecast points combined, the total number of events was 33,012. It should be noted, however, that these events were not entirely independent since an appreciable correlation between these events exists from day to day and from one grid point to another.

Results showed a forecast bias of 1.2 indicating an overall slight tendency to overforecast thunderstorm occurrences. The skill score showed that the operational forecasts were 22 percent better than climatological frequency forecasts.

A desirable characteristic of probability forecasts is that they be reliable. That is, predicted probability should be as close as possible to the observed relative frequency (Sanders, 1967). A plot of the reliability of the operational forecasts for 5 percent intervals is shown in Figure 6. The plot shows that the forecast probabilities closely agreed with the observed frequencies except in the 85 to 100 percent range.

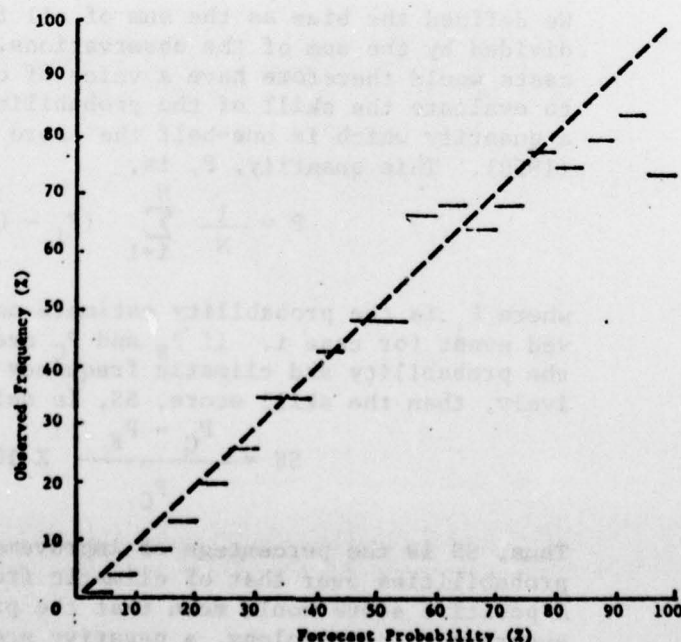


Fig. 6. Reliability of the probability forecasts at 1800 GMT within 5% intervals. Perfect reliability is indicated by the dashed line.

Since these probability forecasts project out only to 6 hr in the future, one might expect persistence to have skill. Out tests showed that persistence fared very poorly in this independent sample, the skill score being inferior to climatology by about 15 percent. This poor performance of persistence is probably due to the short lifetimes of thunderstorms and the diurnal variation in their frequency (Wallace, 1975).

Another way of gaining an insight into the performance of the forecasts is through a series of case studies. Out of seven days picked at random (except for the requirement that thunderstorms must have occurred somewhere in the forecast domain), we chose three cases for verification. The main factor determining our choices was the availability of good verifying MDR data in the areas where the thunderstorms occurred. Thus, the forecasts on the three days selected were not necessarily the best of the original seven.

The probability forecasts and the corresponding verifications for the three cases are shown in Figures 7, 8, and 9. A thunderstorm (or predictand) occurrence was defined in the same way it was in the developmental sample. Therefore, where a T appears the observed pre-

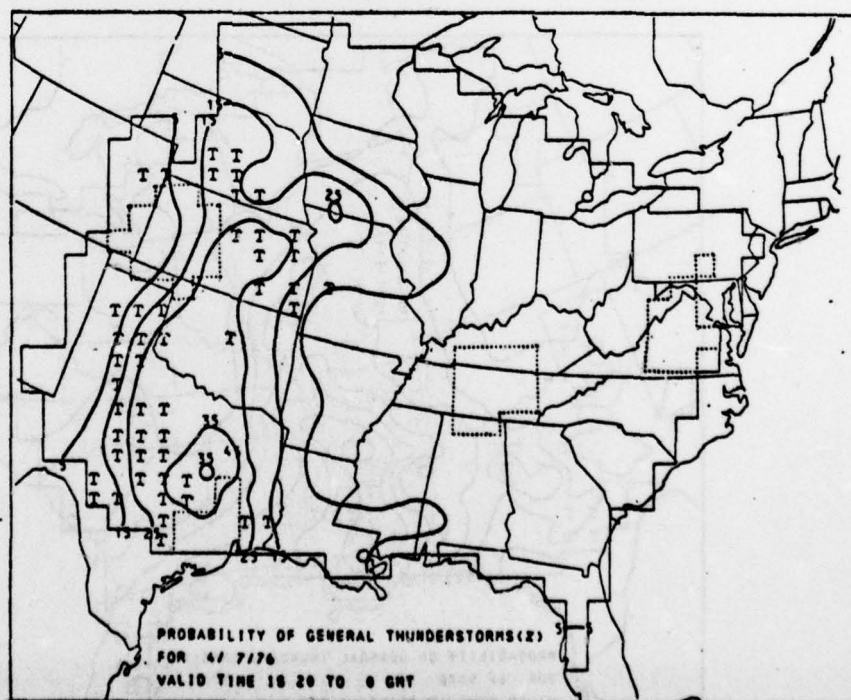


Fig. 7. Sample operational probability forecast with actual occurrences of thunderstorms superimposed. The probabilities were produced by the 1800-GMT primary and backup equations. Thunderstorm occurrences, as determined from MDR data, for the valid period of the forecast are indicated by T's. Within areas enclosed by dotted lines, MDR data were missing and, therefore, verification of the probabilities is not to be considered.

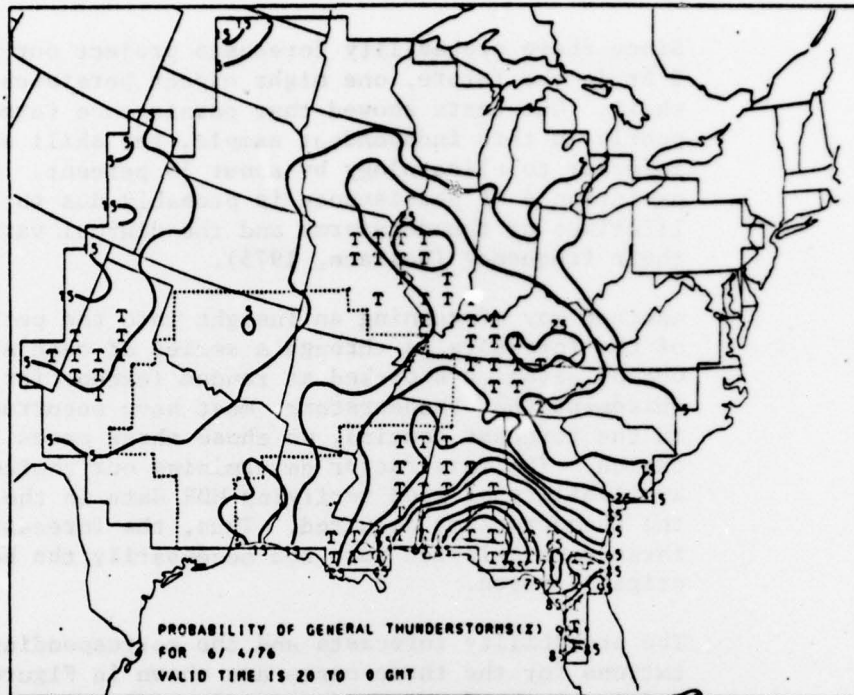


Fig. 8. Same as Fig. 7.

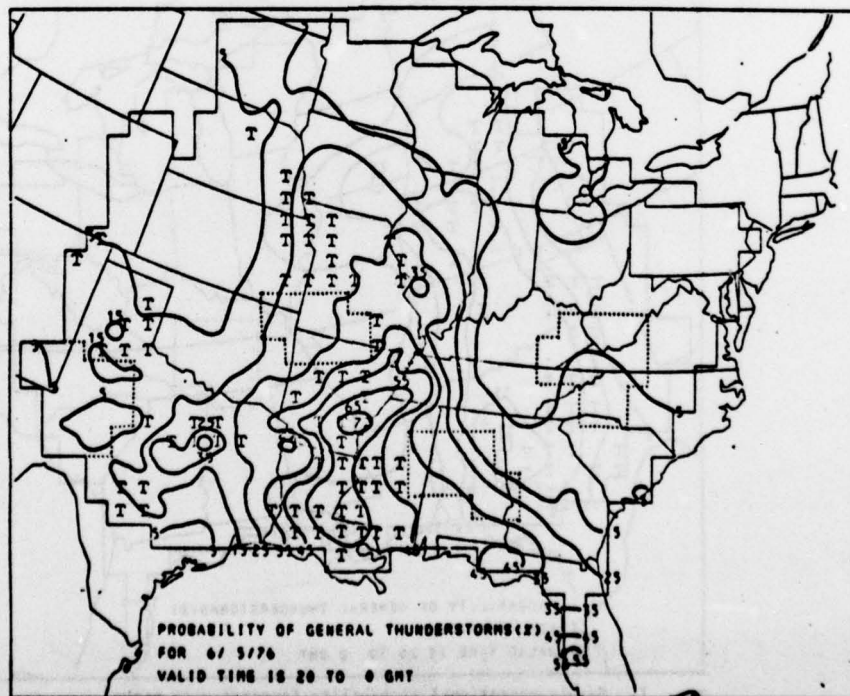


Fig. 9. Same as Fig. 7.

dictand was actually 1; where T's do not appear the predictand was 0. Areas where the verifying MDR data were not available are delineated by dotted lines and should be ignored.

Figures 7, 8, and 9 illustrate that the general pattern of thunderstorm occurrence agrees well with the envelope of higher probabilities. On the other hand, the smaller-scale probability maxima and minima do not verify consistently although they appear to be correct at least as often as incorrect. Another apparent weakness exhibited by these cases is that, when thunderstorms occurred in both the Midwest and along the Gulf Coast, the probabilities were higher in the latter region. This deficiency is likely a consequence of deriving and subsequently applying a single prediction equation for the entire forecasting area. Predictor coefficients and predictor variables appropriate for the Gulf Coastal states are not likely to be the same as for the upper Midwestern states. Therefore, a single equation applied to both regions is likely to result in forecast errors in both regions. Investigation of this problem is currently in progress.

3.3 Future Plans

Our plans call for additional study in several areas which would likely result in improvements to the current forecasts. The following are some of these areas:

- a. Better use could be made of the MDR data. Work, now in progress, shows that the frequency of thunderstorm occurrence (as determined from MDR data) is highly correlated with the distances of the MDR boxes from the radar stations. This distance dependence is due to poor detection of precipitation cells by radar at large ranges from the station. We plan to incorporate procedures which would properly screen poor quality data from the dependent and independent samples.
- b. There are differences in predictor/predictand relationships from one geographical region of the grid to another. These differences are due mainly to the proximity of mountain ranges, large bodies of water, and latitude. Charba (1977b) has successfully accounted for such differences in objective severe local storms forecasting. However, the current thunderstorm forecasting method does not account for them and this is believed to be the cause of geographical biases in the probabilities as noted in the discussion of the case studies. We plan to incorporate techniques which would alleviate this problem.
- c. Another area of investigation which should result in a significant improvement concerns the development of a better method of positioning predictors relative to the

predictand box. In the current procedure, predictors are optimally positioned but only in a climatological sense. It may be profitable to investigate techniques that would position predictors differently for each day according to the synoptic situation.

We can envision the above studies to result in improvements to the current development procedure. Of course, as new data sources and longer data samples become available in the future, these too will result in improving the prediction equations.

4. SUMMARY OF ACHIEVEMENTS

In the 0-2 hr prediction, we have:

- Completed tests and comparisons of 10-, 30-, 60-, and 90-minute forecasts of echo coverage by three different tracking models of varying complexity, from 10- and 30-minute sequences of digitized zero degree reflectivity data. Forecasts were verified over 16 and 64 nmi² areas.
- Tested and compared 10-, 30-, and 60-minute forecasts, by the same models, of vertically integrated liquid water content (VIL) from 10-minute input data sequences. Forecasts were verified over a 16 nmi² area.
- Recommended the most suitable models for different operational applications. The 0-30 minute forecast utilizing CCM may have the accuracy required for use in air traffic control.

In the 2-6 hr prediction, we have:

- Developed thunderstorm probability equations for the period 1700-2100, 2000-0000, and 2300-0300 GMT. Separate equations were derived for the spring and summer seasons.
- Implemented the probability equations on an operational day-to-day basis from April to late September 1976. During this period, the forecasts were transmitted by teletype to NWS and FAA stations by 1540, 1840, and 2140 GMT, respectively.
- Verified the operational probability forecasts against thunderstorm observations.

5. RECOMMENDATIONS

The FAA should adopt the 0-30 minute forecast of thunderstorms for operational tests. These operational tests would lead to procedures on controller use of these forecasts as well as determine the forecast accuracy required for air traffic control.

6. ACKNOWLEDGMENTS

The authors acknowledge with thanks their indebtedness to Mark Jacobs, Steve Chulick, Louis Ruh and Maryrose Loftus for programming assistance, Denis Sakelaris for drafting the figures, and Barbara Howerton and Mary Battle for typing the manuscript.

6. REFERENCES

- Alaka, M. A., W. D. Bonner, J. P. Charba, R. L. Crisci, R. C. Elvander, and R. M. Reap, 1973: Objective techniques for forecasting thunderstorms and severe weather. Final Rep. to Dept. of Transportation, Federal Aviation Administration, Rep. No. FAA-RD-73-117, 97 pp.
- _____, J. P. Charba, and R. C. Elvander, 1975: Short range thunderstorm forecasting for aviation. Interim Rep. to Federal Aviation Administration, Washington, D.C., Rep. No. FAA-RD-75-220, 24 pp.
- Austin, G. L. and A. Bellon, 1974: The use of digital radar records for short term precipitation forecasting. Quart. J. R. Met. Soc., 100, 33-39.
- Barclay, P. A. and K. E. Wilk, 1970: Severe thunderstorm radar echo motion and related weather events hazardous to aviation operations. ESSA Tech. Memo. ERL-NSSL 46, 63 pp.
- Bigler, J. G., R. G. McGrew, and M. St. Clair, 1973: Application of digitizing weather radar data from a four station network. Preprints, 14th Radar Meteor. Conf., Am. Meteor. Soc., Tucson, Arizona, 395-398.
- Blackmer, R. H., Jr., R. O. Duda, and R. Reboh, 1973: Application of pattern recognition techniques to digitized weather radar data. Final Report, Contract 1-36092, SRI Project 1287, Stanford Research Institute, Menlo Park, Cal., 89 pp.
- Brier, G. W., 1950: Verification of forecasts expressed in terms of probability. Mon. Wea. Rev., 78, 1-3.
- Charba, J. P., 1977a: Operational system for predicting thunderstorm probabilities two to six hours in advance. NOAA Tech. Memo (In preparation).
- _____, 1977b: Operational system for predicting severe local storm probabilities two to six hours in advance. NOAA Tech. Memo. (In preparation).
- Cressman, G. P., 1959: An operational objective analysis system. Mon. Wea. Rev., 87, 367-374.
- Donaldson, R. J., Jr., R. M. Dyer, and M. J. Kraus, 1975: An objective evaluator of techniques for predicting severe weather events. Proc. Ninth Conf. on Severe Local Storms, Am. Meteor. Soc., Boston, Mass., 321-326.
- Duda, R. O., and R. H. Blackmer, Jr., 1972: Application of pattern recognition techniques to digitized weather radar data. Final Report Contract 1-36092, SRI Project 1287, Stanford Research Institute, Menlo Park, Cal., 135 pp.

- Elvander, R. C., 1976: An evaluation of the relative performance of three weather radar echo forecasting techniques. Preprints, 17th Radar Meteor. Conf., Am. Meteor. Soc., Boston, Mass., 526-532.
- George, J. J., 1960: Weather Forecasting for Aeronautics. Academic Press, New York, 673 pp.
- Glahn, H. R., and D. A. Lowry, 1972: The use of model output statistics in objective weather forecasting. J. Appl. Meteor., 11, 1203-1211.
- Howcroft, J. and A. Desmarais, 1971: The limited area fine mesh (LFM) model. NWS Tech Proc. Bull. No. 67, 11 pp. (Available from NWS Hqdt., Silver Spring, Md.)
- Klein, W. H., 1970: The forecast research program of the Techniques Development Laboratory. Bull. Am. Meteor. Soc., 51, 133-142.
- Marshall, J. S., and V. M. Palmer, 1948: The distribution of raindrops with size. J. Meteor., 5, 165-166.
- Miller, R. C., 1972: Notes on analysis and severe-storm forecasting procedures for the Military Warning Center. Air Wea. Service, Tech. Rep. 200 (Rev.). Air Force Global Weather Central, Offutt AFB, Neb.
- Miller, R. G., 1964: Regression estimation of event probabilities. Tech. Rep. No. 1 Cwb-10704, The Travelers Research Center, Inc., Hartford Conn., 153 pp.
- Mogil, H. M., 1974: Evaluation of severe weather and thunderstorm forecasts using manually-digitized radar data and SELS severe weather log. Preprints, Fifth Conf. on Weather Forecasting and Analysis, Am. Meteor. Soc., Boston, Mass., 270-275.
- Moore, P. L., A. D. Cummings, and D. L. Smith, 1974: The National Weather Service manually-digitized radar program and its application to precipitation probability forecasting. Preprints, Fifth Conf. on Forecasting and Analysis, Am. Meteor. Soc., Boston, Mass., 266-269.
- Palmer, W. C., and R. A. Allen, 1949: Note on accuracy of forecasts concerning the rain problem. Unpublished manuscript, U.S. Weather Bureau, Washington, D.C., 4 pp.
- Panofsky, H. A., and G. W. Brier, 1958: Some applications of statistics to meteorology. The Pennsylvania State University, University Park, Pa., 224 pp.
- Reap, R. M., and D. S. Foster, 1975: New operational thunderstorm and severe weather probability forecasts based upon model output statistics (MOS). Preprints, Ninth Conf. on Severe Local Storms, Am. Meteor. Soc., Boston, Mass., 58-67.
- Saffie, R. E., 1976: D/RADEX products and field operation. Preprints, 17th Radar Meteor. Conf., Am. Meteor. Soc., Boston, Mass., 555-559.

- Sanders, F., 1967: The verification of probability forecasts. J. Appl. Meteor., 6, 756-761.
- Showalter, A. K., 1953: A stability index for thunderstorm forecasting. Bull. Am. Meteor. Soc., 34, 250-252.
- Shuman, F. G., 1957: Numerical methods in weather prediction: II Smoothing and filtering. Mon. Wea. Rev., 85, 357-361.
- Wallace, J. M., 1975: Diurnal variations in precipitation and thunderstorm frequency over the conterminous United States. Mon. Wea. Rev., 103, 406-419.
- Wilk, K. E. and K. C. Gray, 1970: Processing and analysis techniques used with the NSSL weather radar system. Preprints, 14th Radar Meteor. Conf., Am. Meteor. Soc., Boston, Mass., 369-374.